Electroless Deposition of Metal Nanoislands on Aminothiolate-Functionalized Au(111) Electrodes

Hannes Kind,* Alexander M. Bittner, Ornella Cavalleri, and Klaus Kern

Institut de Physique Expérimentale, École Polytechnique Fédérale de Lausanne, CH-1015 Lausanne, Switzerland

Thomas Greber

Physik-Institut, Universität Zürich, CH-8057 Zürich, Switzerland

Received: March 30, 1998; In Final Form: June 26, 1998

We show that selective electroless deposition (ELD) can be used as a tool for electrochemical nanostructuring. In a first step, we bound palladium ions to an aminothiolate (AT) layer on an Au(111) surface. Chemical reduction then served for the fabrication of metallic palladium islands of monatomic height that can in turn activate the ELD of cobalt. We studied the growth of cobalt islands as a function of the oxygen concentration in the deposition bath and of the aminothiolate concentration in mixed amino-/alkanethiolate self-assembled monolayers (SAMs). In situ scanning tunneling microscopy (STM) and X-ray photoelectron spectroscopy (XPS) measurements showed that palladium and cobalt form islands of 1−3 nm up to 60 nm diameter, the size being controlled by the oxygen concentration in the bath.

1. Introduction

Electroless deposition (ELD) is an autocatalytic redox process in which metal ions are chemically reduced to metal at a surface in absence of any external current source.[1−6] A cation of the metal to be deposited is reduced by receiving electrons from the surface of a metal substrate or from the surface of the catalysts used to initiate the deposition. The reductant in turn delivers electrons to this surface and is thereby oxidized. This redox process generally takes place only on catalytically active metal surfaces: Noncatalytic surfaces first have to be activated with an appropriate catalyst before the metal deposition can take place. The growing metal surface itself has of course to be catalytically active for the process.

The method of ELD has long been used in the electronic industry for the metallization of plastics, ceramics, and other insulating substrates. However, this was based more or less on a trial and error approach. Although several fundamental studies of ELD have been conducted (see, e.g., [refs 2, 3, and 7−9]), the mechanisms of ELD are not fully understood yet. In this paper, we propose ELD on a thiolate surface as model for the metallization of organic substrates.

Our interest in ELD is also related to the patterning of nanometer-sized magnetic objects placed on an organic spacer. The study of ferromagnetism of ultrathin films and small aggregates has shown a very interesting correlation between elastic and magnetic properties.[10] A better study of the magnetism as a function of size and geometry of nanostructures on top of a spacer will allow an interesting comparison with systems without spacers. In our case the thiolate layer should help to minimize any electronic and magnetic interaction between the substrate and magnetic objects on top of the spacer. It will also be possible to study the long-range interaction between different objects.

From an electrochemist's point of view, small aggregates—such as the Pd or Co islands that we investigated—form an ultramicro- or even nanoelectrode array. Such electrodes of geometrical dimension smaller than the Nernst diffusion layer have important advantages pointed out earlier by Ewing et al.[11] They can be used to study fast electron-transfer reactions,[12,13] to perform in vivo voltammetric measurements inside living brain tissue[14] and inside single cells,[14−16] to observe changes in the conductivity of single ion channels,[17] and to perform small-scale etching and lithography.[18] All these applications are mainly based on the fact that redox reaction kinetics and spatial resolution of electrodes scale inversely with the electrode radius, i.e., small currents can be sampled on a small area.[13,19,20]

Metal island nanopatterning requires a selective deposition that can be achieved either by a selective deactivation of a catalytic substrate or by selective activation of an inactive surface by a catalyst.[21] Several methods of producing patterned catalysts are known, often based on photolithographic techniques.[22,23] Other approaches to selective metallization are chemical vapor deposition (CVD)[24] and microcontact printing (μCP).[25−28] Recently direct patterning with a catalyst by MCP of colloids has been demonstrated by Hidber et al.[29]

The resolution of submicrometer metallic features obtained by a selective ELD approach depends on the size of the catalyst particle.[30] Minimal attainable feature line widths will be limited by the largest catalyst particle on the surface.[31] So far the dimensional polydispersity has limited the resolution at which a particular size/shape-dependent characteristic of metal particles may be probed.

Our approach to circumvent this problem is based on the special properties of doubly functionalized molecules. Doubly functionalized self-assembling molecules are very interesting candidates to pattern substrates by MCP.[25−28] While one functional group selectively binds to the surface, the other can be tailor-made to control the external interfacial properties.

* Corresponding author. E-mail: hannes.kind@epfl.ch. Fax: (++41) 21 693 36 04.

S1089-5647(98)01684-8 CCC: $15.00
Published on Web 09/09/1998

Particularly attractive are functionalized thiols that can bind with the sulfur to metal surfaces and form strongly adsorbed, ordered monolayers.[32−34] A variety of metal ion ligands such as pyridine, 2,2′-bipyridine, amine, and ethylenediamine can be used as external functional groups.[22,35,36] Metal ions such as Pd^{2+} (which upon reduction becomes the catalyst Pd^0) can bind to these functional groups. The binding mechanism has been shown to be highly selective for different surface ligands.[37] Hence, the ability to control the strength of the bond between the self-assembled monolayer (SAM) and a catalyst precursor at the molecular level can offer control of the adhesion of the catalyst and hence of metal structures deposited on the catalyst.

We describe here a new method for selective ELD of only one-monolayer thin Pd metal films in which binding of the Pd^{2+} solution species by amine ligands anchors the Pd^{2+} to the organic surface. The reductant (dimethylamine-borane, DMAB) then reduces Pd^{2+} to Pd^0. In a second step we focus on the ELD of nanosized islands of Co on these catalytic sites. Our experimental methods are in situ electrochemical scanning tunneling microscopy (STM) at 300 K, UV spectroscopy of the Pd^{2+} solution and X-ray photoelectron spectroscopy (XPS) of emersed samples.

2. Experimental Techniques

Chemicals. Milli-Q water (18 MΩ resistivity; Millipore Systems) was used for all experiments. All reagents were p.a. grade or better and were used as received. Ethanol, NaCl, Na_4EDTA, NaOH, NH_4Cl, dimethylamine-borane complex (DMAB, $(CH_3)_2NHBH_3$), decanethiol, H_2SO_4, and HCl were all from Fluka. Na_2PdCl_4 and $CoCl_2$ were both from Aldrich Chemical Co. The aminothiol $H_2N(CH_2)_2NHCO(CH_2)_{10}SH$ was used as received from H. Vogel (Institut de Chimie Physique, École Polytechnique Fédérale de Lausanne). Oxygen and nitrogen (48 res. 50 grade from CarbaGas, CH) gases were purified by passage through H_2SO_4 and saturated with H_2O by bubbling through H_2O.

Solutions. Glassware was cleaned with Nochromix solution (Thomas Scientific, U.S.), which reacts violently with many organic materials and should be handled with care. The electroless Co metallization bath was prepared immediately prior to use by mixing three parts of stock Co solution, two parts of stock solution of DMAB, and five parts of H_2O. The Co stock solution was prepared by adjusting a solution of 1 g of NH_4Cl, 0.6 g of $CoCl_2$, and 0.9 g of Na_4EDTA in 100 mL of H_2O to pH = 8 using a 2 M NaOH (aqueous) solution. Stock reductant consisted of a solution of 1.7 g of DMAB in 50 mL of H_2O. Pd^{2+} catalyst solution was prepared of 10 mg of Na_2PdCl_4 and 1.75 g of NaCl in 50 mL of H_2O adjusting the solution with 37% HCl to pH = 1. This yielded the desired $[Pd^{2+}]_{tot}$ of 0.7 mM and $[Cl^-]_{tot}$ of 0.7 M and showed the typical pale yellow color of dilute $PdCl_4^{2-}$ solutions.[38] All solutions were used within 4 weeks.

The pH of the EL Co deposition bath measured over 24 h at room temperature showed that the bath is stable at these conditions. Bubbling of clean nitrogen through the EL plating solution and simultaneous scratching of a pipet against the beaker wall started the bath. A Co layer deposited at the beaker wall was visible to the naked eye. The ELD was always accompanied by the formation of small hydrogen bubbles at the solid/liquid interface.

Substrate Preparation and Monolayer Formation. The gold samples were prepared by evaporation of 120−150 nm 99.99% gold (Advent; Halesworth, U.K.) on 570 K-preheated cleaved mica (Balztec; Vaduz, LIE) in a 10^{-5} mbar vacuum and then annealed for several hours at ∼600 K (2×10^{-6} mbar). Directly before the self-assembly was started, the gold films were flame-annealed at very dark red glow and cooled in ethanol. For the self-assembly, the samples were then quickly transferred into 20 μ**M** ethanolic solutions of the aminothiol. The substrates were left immersed between 17 and 48 h at ∼325 K, thereafter several more days at 300 K. For the experiments with mixed monolayers, the samples were transferred into different mixtures of 20 μM ethanolic solution of the aminothiol and 20 μM ethanolic solution of decanethiol. These substrates were only left immersed 17 h at ∼325 K. All samples were rinsed with ethanol and used immediately.

SCHEME 1: Pd(II) Species in Aqueous Solution

$$PdCl_4^{2-} + H_2O \Leftrightarrow Cl^- + PdCl_3(H_2O)^- \quad (1)$$

$$PdCl_3(H_2O)^- + H_2O \Leftrightarrow Cl^- + PdCl_2(H_2O)_2 \quad (2)$$

$$PdCl_3(H_2O)^- \Leftrightarrow H^+ + PdCl_3(OH)^{2-} \quad (3)$$

$$PdCl_2(H_2O)_2 \Leftrightarrow H^+ + PdCl_2(H_2O)(OH)^- \quad (4)$$

Sample Preparation. The samples were dried in air and then mounted in a PCTFE STM cell, covered by a drop of the Pd^{2+} catalyst solution for 2 min, rinsed three times with H_2O, and finally covered by the Co metallization bath. For XPS analysis the thiolate-covered substrates were rinsed with ethanol and then dipped into the Pd^{2+} catalyst solution for 2 min, rinsed with H_2O, and introduced via a fast entry lock into the vacuum system. All measurements were made at room temperature.

Instrumentation. The STM measurements were performed with a Besocke beetle type STM modified for in situ electrochemical measurements.[39,40] Additionally the microscope was insulated against vibration and electromagnetic fields by an acoustic cabin which at the same time serves as a Faraday cage. The microscope was suspended in the cabin by four elastic strings to suppress the vibrations of the building. All STM images are shown derivatized. Note that the height difference between Au(111), Pd(111), and Co(001) monatomic steps is too small to be detected with our STM. The X-ray photoelectron spectra were collected in a VG ESCALAB 220. To minimize X-ray tube induced damage, the spectrometer transmission was maximized with lowest angular resolution and an overall energy resolution of 1.4 eV fwhm on the Au $4f_{7/2}$ peak at 84.0 eV binding energy. The X-ray twin anode that provides nonmonochromatized Mg Kα (1253.6 eV) radiation was retracted and run with 70 W input power. For all spectra the Au $4f_{7/2}$ peak was set to 84.0 eV binding energy. The emission angles were 0° (normal emission) and 80° (grazing emission). UV-absorption spectra of the Pd^{2+} solutions were obtained using a Shimadzu UV-260 spectrometer.

3. Pd^{2+} Catalyst Experiments

Pd^{2+} Catalyst Solution. Understanding of the Pd^{2+} activation is based on knowledge of the chemical composition of the activation bath. The chemistry of Pd^{2+} halogen complexes in aqueous solution is dominated by hydrolysis above pH ∼ 2[41−44] where hydroxo-and/or chloro-bridged Pd^{2+} oligomers precipitate. The mechanisms that dominate the chemistry in an aqueous solution of $PdCl_4^{2-}$ are shown in Scheme 1. The Cl^- ligands are replaced one after another by H_2O.[45−48] Deprotonation of the hydrolyzed species $PdCl_3(H_2O)^-$ and $PdCl_2(H_2O)_2$ is described by eqs 3 and 4. The resulting hydroxo complexes

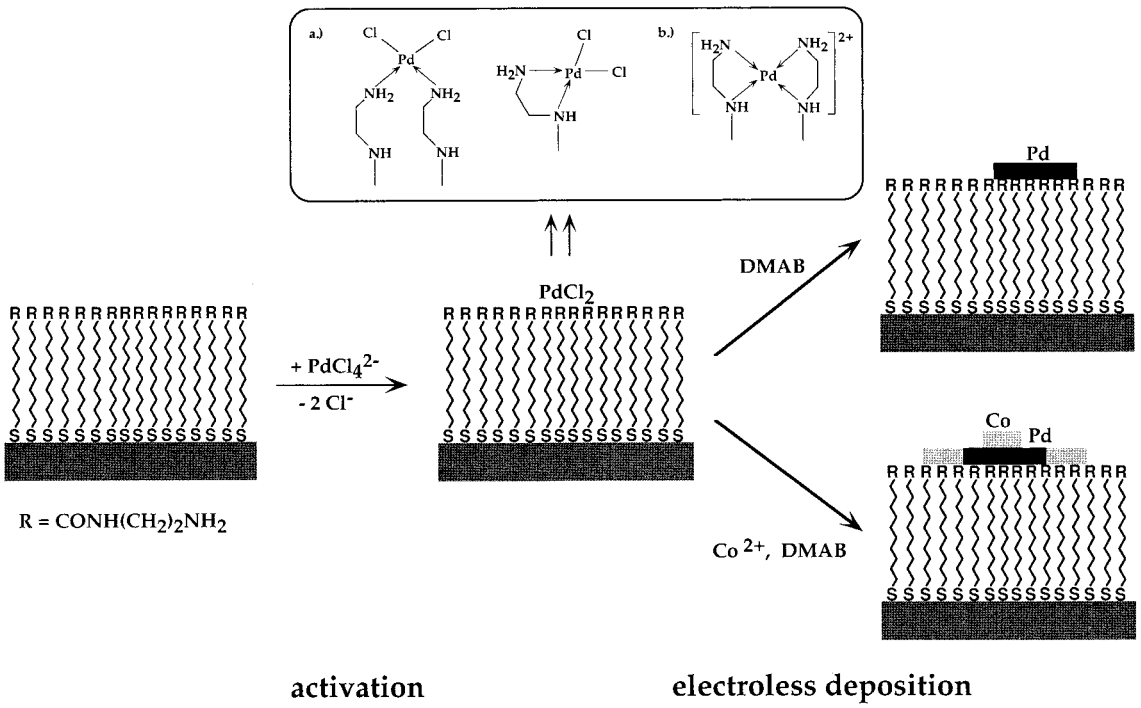

Figure 1. Schematic representation of the ELD of Pd islands and Co/Pd islands. Pd^{2+} binds to the amino groups in the thiolate layer. Dimethylamine-borane (DMAB) reduces Pd^{2+} and Co^{2+} to the respective metals. Possible configurations of the Pd^{2+} bonds with the AT-SAM molecules are shown.

easily lead to the formation of hydroxo- and/or chloro-bridged oligomers.[37,41−44]

Our purpose was to bind only one layer of Pd^{2+} ions (see Figure 1) to the amine-terminated surface. This necessitates that the concentration of hydroxo-and/or chloro-bridged oligomers (for simplicity we call them "Pd nodules" from here on) is kept as low as possible. For this reason we calculated from the reaction constants the required concentration of H^+ and Cl^- to have almost only $PdCl_4^{2-}$ present in the solution.[42,43,47,49,50] In Figure 2 the normalized concentrations of the species are shown for pH = 1 and 5 as a function of the Cl^- concentration. For our experiments we chose a Pd^{2+} solution at pH = 1 with $[Cl^-] = 0.7$ M. In this case the solution contains 86.6% $PdCl_4^{2-}$, 12.4% $PdCl_3(H_2O)^-$, 0.9% $PdCl_2(H_2O)_2$, 1.3×10^{-5}% $PdCl_3(OH)^{2-}$, and 5×10^{-4}% $PdCl_2(H_2O)(OH)^-$ (calculated). A comparison of the corresponding UV spectra (not shown) with spectra obtained by other groups[37,45−48] provides further support that under these conditions $PdCl_4^{2-}$ is indeed the majority species.

Pd^{2+}-Activation Experiments. Let us first focus on the chemical composition of the Pd^{2+}-activated aminothiolate SAM (AT-SAM). An XPS analysis was performed to investigate the vertical position of the Pd^{2+} relative to the monolayer. In Figure 3 Au 4d and Pd 3d XP spectra are shown for grazing (80°) and normal (0°) emission from a Pd^{2+}-activated AT-SAM. The Pd $3d_{5/2}$ peak is clearly visible in grazing emission at ~338.2 eV and corresponds to that of Pd^{2+} bound to nitrogen and/or chlorine.[37] A component at 336 eV that should represent the oxo- or hydroxo-bridged Pd sites in the Pd nodules[37] was never found. In normal emission the Au signal is substantially increased while the Pd signal has disappeared. This can only be explained by a model in which the Pd resides on top of the aminothiolate film.[37]

A comparison of the overview spectra (not shown) of pure AT-SAM showed that the samples are clean and not damaged during the 2 min of Pd^{2+} activation at pH = 1. Furthermore, it was seen from the O ls detail spectra (not shown) that the untreated as well as the Pd^{2+}-treated samples show only minute amounts of oxygen although the second had been exposed to air for more than 30 s. As described elsewhere[39] for alkanethiolate films, we performed X-ray aging experiments for the AT-SAM. Intensity curves for the Au and Pd signal indicate a similar destruction of the AT-SAM with X-ray exposure time. For this reason exposure time was minimized to less than a few minutes.

By varying the Pd^{2+} activation time between 1 and 15 min, we found in STM measurements that the amount of unwanted Pd nodules (not shown) increases with activation time. These nodules are bigger than 20−30 nm in diameter and more than 5−10 monolayers high. Nevertheless we always found flat areas of more than 2.3×10^4 nm^2 free of these nodules. Rinsing of the Pd^{2+}-activated samples with a solution of $[Cl^-] = 0.7$ M at pH = 1 instead of water reduced the number and size of the remaining Pd nodules further. Pd^{2+} activation times between 1 and 2 min were finally determined as best compromise for a sufficient activation without too many Pd nodules. In passing we note that careful rinsing should be sufficient to eliminate all excess Pd species that are not chemically bound to the surface.

Pd^{2+} Reduction Experiments. It is known that only metallic Pd^0 can act as the catalyst for the ELD but not Pd^{2+}. This means that prior to ELD of the metal (in our case Co) the Pd^{2+} species have to be reduced by the reductant (DMAB).

We performed in situ STM measurements to estimate the size and the surface density of such Pd^0 particles. After the activation with Pd^{2+}, the catalyst solution was removed with a pipette; the samples were then carefully rinsed three times with H_2O and were immediately covered by a mixture of two parts of the DMAB stock solution and eight parts of H_2O. A few minutes later the cell was mounted in the STM and measurements were started.

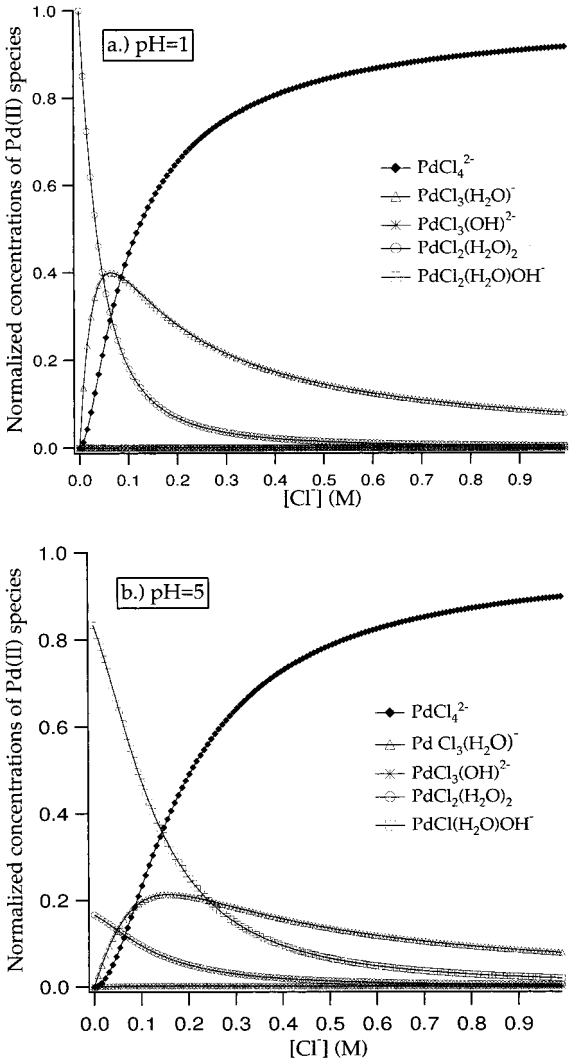

Figure 2. Normalized composition of the Pd^{2+} activation solution at (a) pH = 1 and (b) pH = 5 as a function of $[Cl^-]_{tot}$. The aqueous solution contains Na_2PdCl_4, NaCl, and HC1.

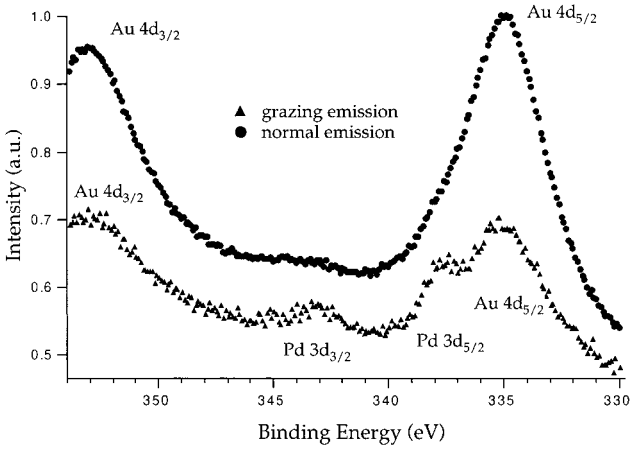

Figure 3. Normal and grazing emission XPS of the Au 4d and Pd 3d core level region of a Pd^{2+}-activated AT-SAM. The increase of the ratio Pd 3d/Au 4f at grazing emission points toward Pd^{2+} on top of the AT-SAM. At normal emission the Pd 3d signal is too low to be resolved.

It has been shown by Dressick et al. that Pd^{2+} particles in the presence of DMAB are completely transformed to Pd^0.[37] In our work we determined shape and density of such Pd^0 particles by STM. Images of the activated surface show that the Pd^0 particles form islands that are homogeneously distributed on the surface (see Figure 4). We only found Pd islands of monatomic height. (The interpretation of a Pd island's height is highly complex since the tunneling mechanism on thiolates and Pd species should be very different. However, a step between a first and a second Pd layer (that we never found) should exhibit the real Pd step height. Further, the steps between the first Pd and the following layers of Co should give an accurate estimate for the Co step height.) The average diameter of the islands was between 1.5 and 6 nm (30−500 Pd atoms per island). Owing to some variability during the Pd^{2+} activation (quality of rinsing with H_2O, contact time with Pd^{2+} solution), the coverage of the surface by the islands varied between 1 and 4%. Assuming a thiolate coverage of typically 1/3 on Au(111) the Pd/NH_2 ratio is between 3 and 12%.

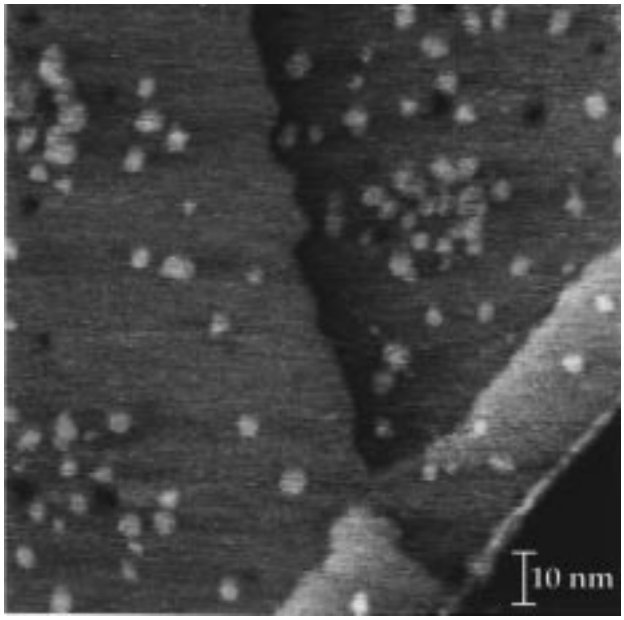

Figure 4. STM image of Pd islands (bright spots) on a Pd^{2+}-activated AT-SAM electrode. The island height is one Pd monolayer. Areas of different gray shades (i.e., different heights) are substrate terraces. Bath: 50 mM DMAB. Tunneling parameters: $I = 1$ nA, $U = 70$ mV.

The reason for the low surface coverage of Pd islands has two origins: First, at pH = 1 a non-negligible amount of amino groups will be protonated which reduces the capability to bind Pd^{2+}. Second, the reduction of the Pd^{2+} species to Pd^0 decreases the strength of the bond to the amino group, and some Pd^0 is probably lost.

4. Electroless Co Deposition Experiments

A prerequisite to understand the ELD on Pd^{2+}-activated AT-SAM is the ELD on a bare metal and a nonactivated AT-SAM surface. After presenting relevant experiments, we focus on Co deposition studies at Pd^{2+}-activated AT-SAMs. Finally we discuss the influence of aminothiolate concentration in mixed aminothiolate/alkanethiolate monolayers and show the dependence of the Co plating on the presence of oxygen.

Electroless Co Deposition on Bare Gold. To test the activity of the Co plating bath we performed an experiment on a gold wire. The gold wire (99.99%) was first cleaned in Nochromix solution, rinsed with H_2O, and finally immersed in a Co plating bath. After 10−20 min, the Co deposit was visible to the naked eye. The deposition could be accelerated either by bubbling nitrogen through the bath or by increasing the bath

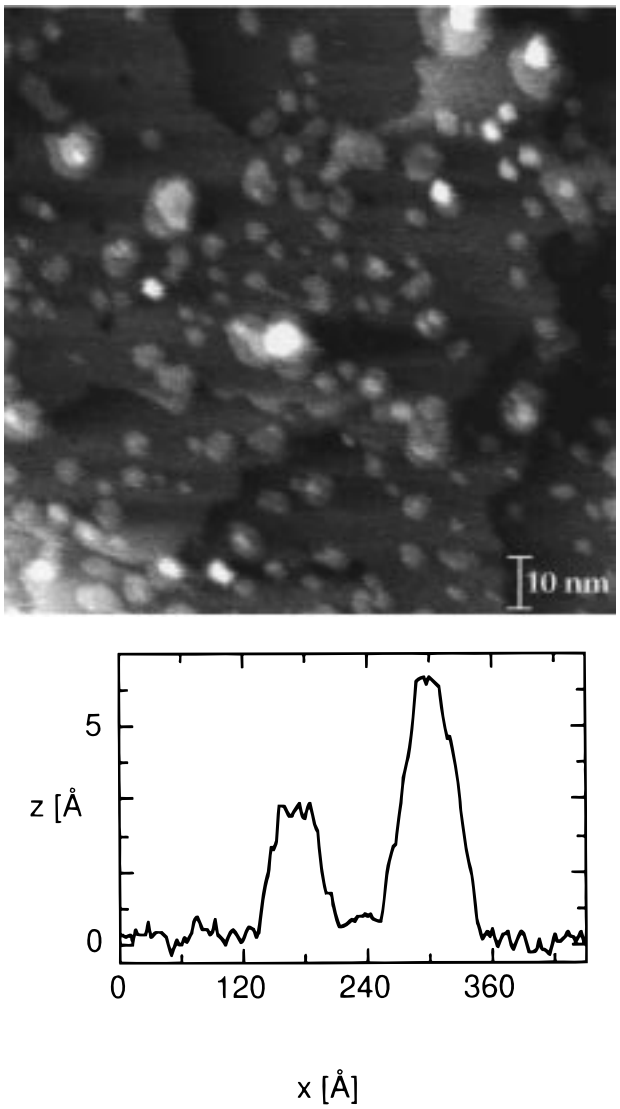

Figure 5. (top) STM image of Co islands on a Pd^{2+}-activated AT-SAM electrode. Bath: 10 mM Co^{2+} + 50 mM DMAB. The brightest islands (e.g. in the right upper corner) contain two or three Co layers. (bottom) Line scan through islands with one (Pd only) and two layers (Pd and Co) measured on an absolute height image (not shown here). Tunneling parameters: I = 0.6 nA, U = 40 mV.

temperature. These Co deposits—a few micrometers thick—could always be dissolved by either HNO_3 or HCl (both of pH = 1) within minutes.

Electroless Co Deposition on Nonactivated AT-SAM. To test the quality of our AT-SAM, we performed in situ STM measurements in the Co plating bath without having activated the AT-SAM with Pd^{2+} solution. We never found any Co deposits on these samples. This agrees well with Dressick's proposition.[22] Furthermore, it proves that we image Co and not contamination. It is important to note that for a Co deposition an activation with the Pd^{2+} solution was absolutely necessary.

Electroless Co Deposition on Pd^{2+}-Activated AT-SAM. After the activation with Pd^{2+} solution, the solution was removed by pipet, samples were then carefully rinsed three times with H_2O, and were immediately covered with the Co plating bath. A few minutes later the cell was mounted in the STM and measurements were started. During the induction time of 10−30 min for our system the Faradaic tip current was too high to perform in situ STM measurements.[6,51] After this period the islands always reached their final size of 1−10 nm diameter

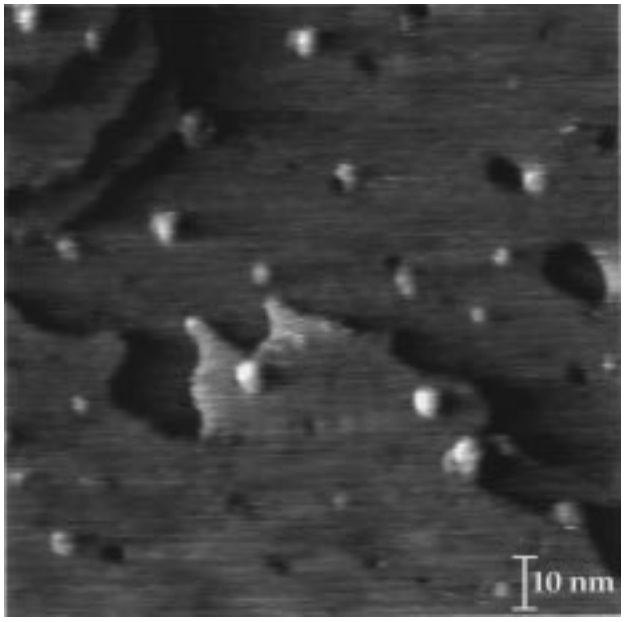

Figure 6. STM image of Co islands on a mixed Pd^{2+}-activated aminothiolate/alkanethiolate-covered Au(111) electrode for a low aminothiolate concentration. Bath: 10 mM Co^{2+} + 50 mM DMAB. The holes are typical for SAMs on Au(111). Tunneling parameters: I = 0.8 nA, U = 40 mV.

and—depending on the sample—one to two (in some rare cases three) Co monolayers height (see Figure 5). Usually the islands were randomly distributed over the terraces and not attached to step edges. In rare cases islands were mainly deposited at step edges. It is very probable that such samples had a lower quality of the SAM. The coverage of the surface by the metallic islands varied between 2 and 20%, again depending on the sample. The variation in island size and surface coverage is mainly attributed to the well-known variability of the SAMs,[39,52,53] the activation time, and the contact to air. Measurements after a few hours and even 24 h later never showed any further growth of the islands. Even a strong increase of either Co^{2+} or DMAB concentration in the plating bath did not influence the island size.

We always found structures similar to that of the above-mentioned Pd nodules. We are sure that these nodules are covered with Co, because also here Pd^{2+} is easily reduced to Pd^0, albeit of unknown structure.

Upon increasing the tunneling current above 2 nA, we could move the islands over the surface, and even downward over steps. Sometimes they coalesced. Such a mobility has never been found for Cu islands electrodeposited on alkanethiolate SAMs, obviously since the latter penetrate into the SAM.[39,54] This gives us further support that the islands are located on top of the monolayer. However, the adhesion of the islands to the surface was strong enough that rinsing with water after the deposition did not remove the islands.

Influence of the Amine Surface Concentration in the SAM. Further proof that the Pd^{2+} species actually bind to the amine ligands was given in experiments where we changed the amino group concentration in the SAM. For this the freshly annealed Au(111) samples were transferred into different mixtures of a 20 μM ethanolic solution of the aminothiol and a 20 μM ethanolic solution of decanethiol. It is well-known[55−57] that in this way the amino group concentration in the SAM can be varied. We changed the ratio aminothiol/alkanethiol in the solution between 2/1 and 1/100. Figure 6 shows a typical image of samples with low or medium amine density. It is obvious

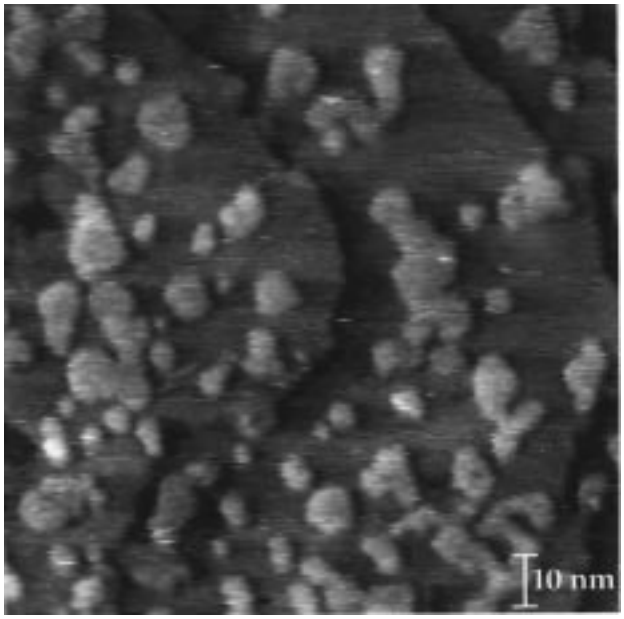

Figure 7. STM image of Co islands on a Pd^{2+}-activated AT-SAM electrode in a bath saturated with nitrogen. Bath: 10 mM Co^{2+} + 50 mM DMAB. The increased island size is obvious from comparison with Figure 5 (no nitrogen), which shows the same scan width. Tunneling parameters: $I = 0.8$ nA, $U = 40$ mV.

that a decreased amine concentration leads to a lower Pd island density and as a consequence also to a lower Co island density. This strongly supports the model of amine-bound Pd^{2+} species. Further we noticed a trend toward smaller islands for decreased amine concentrations (e.g. for aminothiol/alkanethiol = 1/100 the islands were only between 1 and 4 nm in diameter). We deduce from this that we can control the island density and size over a wide range.

Influence of the Oxygen Concentration in the Plating Bath. For a better understanding of the Co growth stop, we performed experiments with plating baths containing either more or less dissolved oxygen than a solution in contact with air.

For this reason we bubbled clean nitrogen through plating solutions for 15 min before use. After a sample was covered by the plating solution, the cell was kept in a nitrogen box for an hour before it was mounted in the STM. However, STM imaging was carried out in the electrolyte in contact to air. Although a dispersion of the results was noticed, there was a clear trend toward islands with a bigger diameter, usually between 3 and 15 nm. A typical image at these conditions is shown in Figure 7. In one case we even found islands of 30−60 nm diameter with 10−20 monolayer height (steps still could be resolved). Generally areas were often completely covered by three-dimensional Co deposits. The poor reproducibility is linked to the not completely controllable contact to air during the sample preparation (e.g. time for the transfer to the nitrogen box).

On the other hand, we repeated the same procedure with a plating solution saturated with pure oxygen and kept under an oxygen atmosphere. For these conditions we noticed that the average size of the island is between 1 and 3 nm, which corresponds well to the values estimated for the pure Pd islands.

We conclude that the growth strongly depends on the oxygen concentration during the ELD. Hence, oxygen addition is an additional control parameter. High oxygen concentrations can prevent Co deposition, while decreased oxygen concentrations cause increased island sizes or even overgrowth of the Pd islands.

5. Discussion

We shall start the discussion with a look at the binding mechanism of the $PdCl_4^{2-}$ ions to the amino groups. $PdCl_4^{2-}$ is the most convenient starting material for many complexes with N ligands and therefore a large collection of chemical and physical data exists.[58,59] Complexes are of the types $[Pdam_4]^{2+}$, $[Pdam_2X_2]$, and $[PdamX_2]_2$ with am = NH_3, amine, 1/2 diamine and X = Cl^-, Br^-, I^-, SCN^-, CN^-. Adding the amine to a solution of $[PdX_4]^{2-}$ under either neutral or acid conditions usually produces $[Pdam_2X_2]$; hence, we expect a similar product when am = aminothiolate. In contrast $[Pdam_4]^{2+}$ is more difficult to prepare.[58]

The inset of Figure 1 shows the different possible configurations of the *N*-(2-aminoethyl)amide end group of the AT-SAM. Mainly three factors determine the binding process at our interface: chelate effect and steric and electrostatic repulsion. Concentrating on these effects, case b is not very likely because Pd^{2+} would have to penetrate into the layer, which would be followed by a strong increase of steric and electrostatic repulsion between the neighboring Pd^{2+}-aminothiolate entities. For this reason it is more likely that complexes in Figure 1d will exist at the interface. This is supported by the fact that a chelate effect occurs and that steric and electrostatic repulsion are minimized.

For a better understanding of the island formation, we want to focus now on the binding energies between Pd and N before and after the reduction of the Pd^{2+} species. First, we calculated approximately the Pd^{2+}−N binding energy from thermodynamical data[60] to be ∼1.5 eV (the Pd^{2+}−Cl binding energy was estimated to be ∼2.1 eV).

Pd^0−N complexes could not be found in the literature (stable Pd^0 complexes can be formed with, e.g., As-, Sb-, or P-containing ligands[58]). The reason can be explained by the ligand-field theory. The electron configuration of Pd^0 is d^{10} and shows very unfavorable energetics compared to the Pd^{2+} configuration which is d^8 (the stabilization of $-24.56\ D_{q0}$ with a ligand field stabilization energy $D_{q0} > 0.15$ eV[61] is larger than a typical chemical bond energy). Therefore the Pd^0−N bond must be much weaker than the Pd^{2+}−N bond, and thus the Pd^0 species can diffuse over the surface.

Calculating, on the other hand, the Pd−Pd bond energy in bulk metal, we found 3.9 eV for a macroscopic Pd solid.[60] Calculations with an effective medium code[62] estimated the bond energy for a Pd atom in a Pd(111) island containing 16 atoms to be ∼3 eV. In both cases (microscopic and macroscopic) the Pd−Pd bond energy is twice as high as the Pd^{2+}−N binding energy. This favorable situation allows the formation of stable Pd islands.

We propose here a model where the Pd^{2+} entities are distributed homogeneously over the surface. They are then first reduced by the reductant to Pd atoms. During the reduction, the strength of the Pd−N bond is lowered and Pd atoms can diffuse over the surface. Nucleation and growth of the Pd atoms results in stable islands.

Let us now concentrate on the discussion of the Co growth stop. It is necessary to consider the oxidation of the reductant

(eq 1), cathodic reduction of the metal ion (eq 2), and oxygen reduction (eq 3):

$$j(\text{Red}): \quad \text{Red} \leftrightarrow \text{Ox} + me^- \tag{1}$$

$$j(M^{n+}): \quad M^{n+} + ne^- \leftrightarrow M \tag{2}$$

$$j(O_2): \quad O_2 + 2H_2O + 4e^- \leftrightarrow 4OH^- \tag{3}$$

The influence of H^+ reduction will be discussed later. The competition between reactions 1 and 3 determines whether the metal will be deposited.[63] For our system all partial reactions can take place first at Pd and later at Co. Thus, the overall reaction is highly complex.[64,65] (In fact, the partial reactions of ELD can occur at different places. One can envisage that the electrons move from the adsorbed reductant through Pd and Co islands to another site where Co^{2+} is reduced. In our case, electrons can even move from one metal island to another metal island via the Au substrate since electrons are rapidly transferred through thiolate layers.[39,66])

As mentioned above, the islands always reached their final size before the first in situ STM measurement was performed. This means that the growth had stopped within a few minutes. To our knowledge a growth extinction has been found before by two other groups. Jacobs et al. found a lower limit to the size of nuclei below which ELD does not occur or is stopped after a short time.[63] They explained the growth stop with an enhanced nonlinear oxygen diffusion under the assumption that the diffusionally limited rate of oxygen reduction $j(O_2)$ is larger than that of the kinetically controlled oxidation of the reducing agent j(Red). A further decrease in the electrode dimensions down to some 10 nm is equivalent to an increase in the mass transport of reactants relative to the rate of electron transfer. Thus, reactions that are limited by diffusion at mesoscopic and macroscopic electrodes can become limited by the rate of the electron transfer as the electrode size is reduced,[63] but $j(O_2) > j$(Red) will still be assured. For completeness it has to be mentioned that $j(O_2)$ at electrodes below 10 nm is no longer controlled by diffusion but by kinetics.[67] This can reduce the expected current (calculated for a purely diffusion controlled mechanism) by a factor of 3−5. Nevertheless, this will not change that $j(O_2) > j$(Red).

Van der Putten et al.[21,68] showed that—depending on the exact conditions—the nonlinear diffusion can lead both to an enhanced local growth or to no growth at all. The latter is possible if a compound is added that can be reduced at more anodic potentials than the metal ion reduction, e.g., dissolved oxygen in the plating bath. Although Van der Putten's model was only confirmed for electrodes in the micrometer range, the similarity of the shape of our islands with their pyramid-like structures is striking. We always found very few islands with three monatomic high terraces, some more with two, and a great majority had only one terrace.

Moreover, we estimated $j(O_2)$ on Pd and Co.[63,69] Both values are of the same order of magnitude and do not explain the growth stop of Co (a reasonable explanation would be $j(O_2)_{Co} \gg j(O_2)_{Pd}$: After the Pd island is covered with Co, $j(O_2)_{Co}$ would consume all electrons delivered by the reductant and the growth would cease).

Another problem is the hydrogen evolution during the plating. Van der Meerakker stated that hydrogen evolves during almost all electroless reactions and proposed a general mechanism based on the formation of atomic hydrogen during the oxidation of the reducing agents.[65] During our experiments we observed small hydrogen bubbles at the liquid/solid interface. This will influence the ELD. It is known that the H^+ reduction is faster on Pd than on Co. That means that the Pd islands may be partly covered by H (or even transformed to Pd hydride), which can influence further metal deposition.

Concentrating on the described effects, we have to conclude that it is very difficult to reach a final conclusion on the stop of the growth. Nevertheless, we want to stress that the oxygen in the deposition bath is the main parameter to control the island size and thus likely to be responsible for the growth stop. We are certain that in our case nonlinear oxygen diffusion controls the deposition at the molecular level.

5. Conclusions

Pd can be grown by electroless deposition (ELD) in nanometer-sized islands on self-assembled aminothiolate layers (AT-SAMs) on Au(111) electrodes. They can be investigated by in situ STM. The most likely place of the Pd is on top of the AT-SAM as proven by normal and grazing emission angle X-ray photoelectron spectroscopy, by the fact that they can be moved by slightly increasing the tunneling current, and finally by the strong correlation with the amine surface concentration in mixed monolayers. The Pd island density can be varied over a large range by changing the amine concentration in a aminothiolate/alkanethiolate SAM.

On these Pd islands nanometer-sized Co islands can be deposited via ELD. The size of such islands can be controlled by the oxygen concentration in the Co plating bath. Processes causing the stop of the island growth were discussed.

Our concept to fabricate nanometer-sized islands of Co and Pd should be applicable to many magnetic and nonmagnetic metals. In combination with microcontact printing to pattern the AT-SAM, it should be possible to fabricate diverse metal cluster arrays.

Acknowledgment. We thank H. Vogel for providing the aminothiol and H. Brune for his help with the effective medium calculation. A.M.B. would like to express his gratitude to the Alexander von Humboldt-Stiftung for a Feodor-Lynen-Stipendium.

References and Notes

(1) Weber, C. J.; Pickering, H. W.; Weil, K. G. In preparation.
(2) Paunovic, M. *Proc. Symp. Electroless Deposition Met. Alloys* **1988**, *88*, 3.
(3) Shipley, C. R. *Plat. Surf. Finish.* **1984**, *71*, 92.
(4) Molenaar, A. *Proc. Symp. Electroless Deposition Met. Alloys* **1988**, *88*, 37.
(5) Okinaka, Y.; Osaka, T. *Electroless Deposition Processes: Fundamentals and Applications*; VCH: Weinheim, 1990.
(6) Weber, C. J.; Pickering, H. W.; Weil, K. G. *J. Electrochem. Soc.* **1997**, *144*, 2364.
(7) Osaka, T.; Takematsu, H. *J. Electrochem. Soc.* **1980**, *127*, 1021.
(8) Besenhard, J. O.; Krebber, U.; Hoerber, J. K.; Kanani, N.; Meyer, H. *J. Electrochem. Soc.* **1989**, *136*, 3608.
(9) Mallory, G. O. *Electroless Plating: Fundamentals and Applications;* American Electroplaters and Surface Finishers Society: Orlando, FL, 1990.
(10) Sander, D.; Skomski, R.; Schmidthals, C.; Enders, A.; Kirschner, J. *Phys. Rev. Lett.* **1996**, *77*, 2566.
(11) Ewing, A. G.; Dayton, M. A.; Wightman, R. M. *Anal. Chem.* **1981**, *53*, 1842.
(12) Morris, R. B.; Franta, D. J.; White, H. S. *J. Phys. Chem.* **1987**, *91*, 3559.
(13) Penner, R. M.; Heben, M. J.; Longin, T. L.; Lewis, N. S. *Science* **1990**, *250*, 1118.
(14) Ewing, A. G.; Wightman, R. M.; Dayton, M. A. *Brain Res.* **1982**, *249*, 361.
(15) Tanaka, K.; Kashiwagi, N. *Bioelectrochem. Bioenerg.* **1987**, *17*, 519.

(16) Tanaka, K.; Kashiwagi, N. *Bioelectrochem. Bioenerg.* **1989**, *21*, 95.
(17) Conti, F.; Neher, E. *Nature* **1980**, *285*, 140.
(18) Craston, D. H.; Lin, S. W.; Bard, A. J. *J. Electrochem. Soc.* **1988**, *135*, 785.
(19) Bard, A. J.; Faulkner, L. R. *Electrochemical Methods: Fundamentals and Applications*; John Wiley & Sons: New York, 1980.
(20) Fleischmann, M.; Lasserre, F.; Robinson, J.; Swan, D. *J. Electroanal. Chem.* **1984**, *177*, 97.
(21) Van der Putten, A. M.; de Bakker, J. W. *J. Electrochem. Soc.* **1993**, *140*, 2229.
(22) Dressick, W. J.; Dulcey, C. S.; Georger, J. H.; Calvert, J. M. *Chem. Mater*. **1993**, *5*, 148.
(23) Vargo, T. G.; Gardella, J. A.; Calvert, J. M.; Chen, M. S. *Science* **1993**, *262*, 1711.
(24) Potochnik, S. J.; Pehrsson, P. E.; Hsu, D. S.; Calvert, J. M. *Langmuir* **1995**, *11*, 1841.
(25) Kumar, A.; Whitesides, G. M. *Appl. Phys. Lett.* **1993**, *63*, 2002.
(26) Kumar, A.; Biebuyck, H. A.; Whitesides, G. M. *Langmuir* **1994**, *10*, 1498.
(27) Xia, Y.; Whitesides, G. M. *Angew. Chem., Int. Ed.* **1998**, *37*, 550.
(28) Delamarche, E.; Schmid, H.; Bietsch, A.; Larsen, N. B.; Rothuizen, H.; Michel, B.; Biebuyck, H. *J. Phys. Chem. B* **1998**, *102*, 3324.
(29) Hidber, P. C.; Helbig, W.; Kim, E.; Whitesides, G. M. *Langmuir* **1996**, *12*, 1375.
(30) Brandow, S. L.; Dressick, W. J.; Marrian, C. R.; Chow, G. M.; Calvert, J. M. *J. Electrochem. Soc.* **1995**, *142*, 2233.
(31) Marrian, C. R.; Perkins, F. K.; Brandow, S. L.; Koloski, T. S.; Dobisz, E. A.; Calvert, J. M. *Appl. Phys. Lett.* **1994**, *64*, 390.
(32) Nuzzo, R. G.; Zegarski, B. R.; Dubois, H. *J. Am. Chem. Soc.* **1987**, *109*, 733.
(33) Bryant, M. A. *J. Am. Chem. Soc.* **1991**, *113*, 8284.
(34) Camillone, N.; Chidsey, C. E.; Liu, G.-Y.; Scoles, G. *J. Chem. Phys.* **1993**, *98*, 4234.
(35) Calvert, J. M.; Calabrese, G. S.; Bohland, J. F.; Chen, M. S.; Dressick, W. J.; Dulcey, C. S.; Georger, J. H.; Kosakowski, J.; Pavelcheck, E. K.; Rhee, K. W.; Shirey, L. M. *J. Vac. Sci. Technol. B* **1994**, *12*, 3884.
(36) Calvert, J. M. *J. Vac. Sci. Technol. B* **1993**, *11*, 2155.
(37) Dressick, W. J.; Dulcey, C. S.; Georger, J. H.; Calabrese, G. S.; Calvert, J. M. *J. Electrochem. Soc.* **1994**, *141*, 210.
(38) Van der Putten, A. M.; de Bakker, J. W.; Fokkink, L. G. *J. Electrochem. Soc.* **1992**, *12*, 3475.
(39) Cavalleri, O.; Bittner, A. M.; Kind, H.; Kern, K.; Greber, T. *Z. Phys. Chem.*, in press.
(40) Gilbert, S. E.; Cavalleri, O.; Kern, K. *J. Phys. Chem.* 100, 12123 1996.
(41) Wyatt, I. R. *Chem. Weekbl.* **1966**, *62*, 310.
(42) Kazakova, V. I.; Ptitsyn, B. V. *Russ. J. Inorg. Chem.* **1967**, *12*, 323.
(43) Nabivanets, B. I.; Kalabina, L. V. *Sov. Prog. Chem.* **1975**, *41*, 81.
(44) Nabivanets, B. I.; Kalabina, L. V. *Russ. J. Inorg. Chem.* **1970**, *15*, 818.
(45) Elding, L. I. *Inorg. Chim. Acta* **1972**, *6*, 683.
(46) Elding, L. I. Olssen, L. F. *J. Phys. Chem.* **1978**, *82*, 69.
(47) Bekker, P. Z.; Robb, W. *J. Inorg. Nucl. Chem.* **1975**, *37*, 829.
(48) Vargaftik, M. N.; Igoshin, V. A.; Syrkin, Y. K. *Izv. Akad. Nauk SSSR, Ser. Khim.* **1972**, *6*, 1426.
(49) Rund, J. V. *Inorg. Chem.* **1970**, *9*, 1211.
(50) Maitlis, P. M. *The Organic Chemistry of Palladium-I. Metal Complexes*; Academic Press: New York, 1971.
(51) Haruyama, S.; Ohno, I. *Proc. Electrochem. Depos. Thin Films* **1993**, *93*, 70.
(52) Sondag-Huethorst, J. A.; Fokkink, L. G. *Langmuir* **1995**, *11*, 4823.
(53) Camillone, N.; Leung, T. Y.; Scoles, G. *Surf. Sci.* **1997**, *373*, 333.
(54) Cavalleri, O. Ordering and electrodeposition at the alkanethiol/Au-(111) interface. Ph.D. Thesis, EPF Lausanne, 1997.
(55) Bain, C. D.; Evall, J.; Whitesides, G. M. *J. Am. Chem. Soc.* **1989**, *111*, 7155.
(56) Delamarche, E.; Michel, B.; Biebuyck, H. A.; Gerber, C. *Adv. Mater.* **1996**, *8*, 719.
(57) Takami, T.; Delamarche, E.; Michel, B.; Gerber, C. *Langmuir* **1995**, *11*, 3876.
(58) Livingstone, S. E. *Comprehensive Inorganic Chemistry*; Bailor, K., Ed.; Pergamon Press: Oxford, 1973; Vol. 3.
(59) Baes, C. F.; Mesmer, R. E. *The Hydrolysis of Cations*; Wiley-Interscience: New York, 1976.
(60) Mortimer, C. T. *Rev. Inorg. Chem.* **1984**, *6*, 233.
(61) Huheey, J. E. *Inorganic Chemistry: Principles of Structure and Reactivity*; Harper Row: New York, 1983.
(62) Stoltze, P. *Condens. Mater.* **1994**, *6*, 9495.
(63) Jacobs, J. W.; Rikken, J. M. *J. Electrochem. Soc.* **1988**, *135*, 2822.
(64) Wiese, H.; Weil, K. G. *J. Electroanal. Chem.* **1987**, *228*, 347.
(65) Van der Meerakker, J. E. *J. Appl. Electrochem.* **1981**, *11*, 395.
(66) Smalley, J. F.; Feldberg, S. W.; Chidsey, C. E.; Linford, M. R.; Newton, M. D.; Liu, Y. P. *J. Phys. Chem.* **1995**, *99*, 13141.
(67) Seibold, J. D.; Scott, E. R.; White, H. S. *J. Electroanal. Chem.* **1989**, *264*, 281.
(68) Van der Putten, A. M.; de Bakker, J. W. *J. Electrochem. Soc.* **1993**, *140*, 2221.
(69) Meruva, R. K.; Meyerhoff, M. E. *Anal. Chem.* **1996**, *68*, 2022.